PERGAMON

International Journal of Multiphase Flow 26 (2000) 1209–1234

International Journal of Multiphase Flow

www.elsevier.com/locate/ijmulflow

Development of a new spray/wall interaction model

Seong Hyuk Lee[a], Hong Sun Ryou[b,*]

[a] *Research Institute of Production Engineering, ChungAng University, Seoul, South Korea*
[b] *Department of Mechanical Engineering, ChungAng University, Seoul, South Korea*

Received 30 July 1998; received in revised form 28 June 1999

Abstract

This paper deals with the development and testing of a new spray/wall impingement model, which is based on the energy conservation law and experimental considerations. A new formula for the viscous dissipated energy of the film is derived in the present investigation to determine the viscous dissipation process of the film in the energy conservation law. In addition, the tangential behavior of droplets after impingement is determined by the newly proposed model, which incorporates both the kinematic parameters of the impinging droplets and the fluid properties. The new model consists of three representative regimes such as rebound, deposition and splash from experimental considerations. To assess the new model, the numerical calculation for several experimental conditions are carried out for the non-evaporative impinging sprays on a flat wall. The numerical results using the new model are compared with the experimental data and the results of the previous impingement models. The results show that the new model generally predicts the splash behavior better than the previous models, and it performs for prediction of local droplet velocities and size effectively, relative to the previous models. Therefore, it can be concluded that the new model is acceptable for predicting the non-evaporative sprays impinging on the wall.

Keywords: Impingement; Wall spray; Splash; Deposition; Direct injection

1. Introduction

Droplet impingement on a solid wall is a phenomenon encountered in a wide variety of fields such as spray cooling, ink jet printing, soil erosion by rain and in direct injection (DI)

* Corresponding author. Tel.: +82-282-05280; fax: +82-2816-4972.
E-mail address: cfdmec@cau.ac.kr (H.S. Ryou).

0301-9322/00/$ - see front matter
PII: S0301-9322(99)00080-4

engines. Particularly in recently developed compact high-speed DI diesel engines, spray impingement on walls appears unavoidable. During cold starting, the low gas pressure facilitates spray penetration and results in the formation of fuel-rich zones close to the wall surface, leading to incomplete combustion with consequently high levels of unburned hydrocarbons and soot particles in the exhaust gases. Gonzalez et al. (1991) have argued that spray impingement was an important factor in cold start. According to their results, the smoke levels have been shown to increase during cold start as a result of the accumulation of fuel on the wall. Therefore, a better understanding of the droplet behavior and fuel dispersion process on the wall will help in designing injection and control systems to improve engine performance and to control emissions.

Generally, spray impingement phenomena are difficult to analyze through experiments under engine operating conditions. Most experiments are dependent on the photographic means in specially adapted engines, as in Ref. (Winterbone et al., 1994), and also in this way the details of useful data are very restricted. Hence, it is extremely difficult to measure droplet size and velocity distributions in the near-wall region. Computational modeling offers a promising alternative for the purpose of obtaining detailed information on spray impingement characteristics.

Recently, several droplet impingement submodels for use in numerical simulations have been developed for describing the interaction between droplets and the wall. Naber and Reitz (1988) have developed a model to study spray impingement using the KIVA code. In their model, there are three regimes, i.e. stick model, in which impinging droplets are stick on the wall, rebound model, in which those are reflected elastically, and finally jet model assuming that after impingement, droplets are moving along the wall surface with the same velocity magnitude before impingement. The main problem in this model is to ignore the phenomenon of droplet shattering occurring at high collision energy and the loss of momentum and energy of the impinging droplets. Watkins and Wang (1990) and Park (1994) have proposed submodels, which differ from the model of Naber and Reitz (1988). The transition criterion of both models between the rebound and scattering regime is described by Weber number of 80 deduced from experimental data of Wachters and Westerling (1966) on water droplets impinging with a very hot wall whose temperature is above the Leidenfrost temperature of the fuel. The difference between both models is that the model of Park (1994) determines the tangential and normal velocity of ejected droplets using the relationship deduced from experimental data, and considers the variation of droplets after impingement. However, the criterion using in both models is not applicable to a wall whose temperature is below the fuel boiling temperature. Hence, the results of both models were found to significantly under-predict the dispersion of sprays away from the wall when compared to experimental data (Watkins and Wang, 1990; Park, 1994; Park and Watkins, 1996). In particular, the model of Park (1994) has not appropriately predicted the splash effect because it has been modeled on the basis of the hot wall data. To reflect the splash regime or dispersion of droplets effectively, Bai and Gosman (1995) have developed methodology on the basis of results on the literature on single droplet impingement and the conservation laws. In addition, Stanton and Rutland (1996) have proposed a submodel involving the splash effect and liquid film model. However, in the above models the angle of ejected droplets is determined from consideration of experimental data. For example, in the Bai and

Gosman model, the ejection angle is randomly chosen in the range from 5° and 50° while, in the Stanton and Rutland model, it is uniformly determined from linear interpolation of the experimental data obtained by Mundo et al. (1995).

The aim of the present study is to propose a new model for impinging droplets on a cold and wetted wall below the fuel boiling temperature, and to test the model for several experimental conditions. In the present study, the 'cold wall' means one with the temperature below the fuel boiling point. The new model based on the conservation law and experimental results consists of three representative regimes such as rebound, deposition and splash. The regime transition criterion between deposition and splash is determined by the empirical correlation proposed by Mundo et al. (1995) and represented as a function of the droplet Reynolds number and Ohnesorge number. From the energy conservation law of primary and secondary droplets, we can determine total velocities of droplets, which leave the wall. Yarin and Weiss (1995) have shown theoretically that the splashing threshold corresponds to the onset of a velocity discontinuity propagating over the liquid layer on the wall. In the new model, the tangential velocities of splashing droplets are obtained from a theoretical relationship considering the kinematic discontinuity. Finally, the angle of splashed droplets can be determined by using this relation and the energy conservation law. Numerical simulations are performed for the non-evaporative impinging sprays on a wall to validate the new model. In addition, the calculated results are compared with experimental data and the predictions using the previous models of Park (1994) and Watkins and Wang (1990). As a whole, it is found that the results of the new model are in better agreement with the experimental data than those of the models of Park (1994) and Watkins and Wang (1990). In particular, the new model can effectively capture the splash effect of ejected droplets after impingement. Therefore, it can be concluded that the new model proposed in this article may be acceptable for prediction of the impinging sprays on walls.

Table 1
Previous impingement models

Rebound regime ($We_{bn} < 80$)	Breakup regime ($We_{bn} > 80$)
The model of Watkins and Wang (1990)	
$D_a = D_b$	$D_a = 0.25 \cdot D_b$
$v_{at} = \sqrt{1 - 0.95\cos^2\beta} \cdot v_{bt}$	$v_{at} = v_{bt}$
$v_{an} = \sqrt{1 - 0.95\cos^2\beta} \cdot v_{bn}$	$v_{an} = 0$
$N_a = N_b$	$N_a = N_b$
The model of Park (1994)	
$D_a = D_b$	$D_a^1 = D_a^2 = D_b / N_{eject}^{0.333}$
$v_{at} = v_{bt}$	$v_f^1 = v_f^2 = 0.835(3.096 - 2\xi)v_{bn}$
$v_{an} = \sqrt{1 - \kappa\cos^2\beta} \cdot v_{bn}$	$v_{an} = \sqrt{1 - \kappa\cos^2\beta} \cdot v_{bn}$
$N_a = N_b$	$N_a^1 = N_a^2 = N_b \cdot N_{eject}/2$
	where ξ: model constant

2. Impingement models

2.1. Previous impingement models

The models of Watkins and Wang (1990) and Park (1994) are adopted to assess the new model developed in the present work and to compare the characteristics of impingement models. These previous models listed in Table 1 have been based on the hot wall data performed by Wachters and Westerling (1966). In the model of Park (1994), ξ is the model constant that represents the fraction of the time, which occur the film breakup, and can be varied from 1.0 to 1.28 for low and high velocity, respectively. In particular, in the Park's model, an incident droplet parcel is separated into two parcels with same diameter and velocity of droplets after impingement for $We_{bn} > 80$. Subscripts b and a represent the state before and after impingement, respectively, and n and t are the normal and tangential components, respectively. Also, the superscripts 1 and 2 denote the identity of two separated parcels. In the model, κ is the coefficient for the loss of energy, determined by Wachters and Westerling (1966). After impingement, the number of droplets in an ejected droplet parcel can be determined by using experimental data of Naber and Farrell (1993).

Naber and Farrell (1993) concluded that for diesel engines, where the normal in-cylinder surface temperature range from 400 to 600 K, the appropriate hydrodynamic regime is the wetting regime. Bai and Gosman (1995) and Eckhause and Reitz (1995) have also referred the situation of typical DI diesel engines as the wetting regime. Particularly, in DI diesel engines, the formation of emissions of unburned hydrocarbons and soot particles dominantly occurs in the cold start situation rather than in operating situation because there are incomplete combustion, resulting in the deposit of fuel film formed on the wall surface. Therefore, we can point out that the previous models are not suitable for DI diesel engines of the surface temperature below the critical temperature because the models use the regime criterion based on the experimental data on a non-wetting regime. In addition, none of these models accounts for partial deposition, film existing at the wall, energy dissipation of the film and the splash effect effectively because there are no physical bases on the splash mechanism and the transient behavior of film deposited on the wall. Also, it can be regarded as the weakness of these models that the experimental results on which these models are dependent are not suitable for the splash phenomena.

2.2. The new impingement model

The newly proposed model in the present study is devised to represent the situation involving wall temperatures below the fuel boiling point as is typical DI diesel engines, consistent with Naber and Farrell's (1993) observation. It may be noted, therefore, that the new model that Leidenfrost effects are not included may not hold for low-heat-rejection diesel engines where Leidenfrost effects exist. In the new model, there are three regimes such as rebound, deposition and splash. To begin with, the rebound regime occurs when the impinging droplet bounces off the film when the impingement energy is low. The transition criterion between deposition and rebound is given as Weber number of 5 from the work of Bai and Gosman (1995). In rebound regime where Weber number of an incident droplet is smaller than

5, the velocity of the rebounding droplet is determined by using the method developed by Matsumoto and Saito (1970) for small particles bouncing on a wetted surface, as follows:

$$v_{at} = \frac{5v_{bt}}{7} \tag{1}$$

$$v_{an} = -ev_{bn} \tag{2}$$

where e is the coefficient of restitution that can be determined by using Eq. (3) as reported by Bai and Gosman (1995).

$$e = 0.993 - 1.76\theta_i + 1.56\theta_i^2 - 0.49\theta_i^3 \tag{3}$$

where θ_i represents the incident angle of impinging droplets measured from the wall surface. Mundo et al. (1995) have investigated multi-droplet impingement on rough surfaces and found the criterion between the deposition and splash regime. In the new model, the deposition-splashing boundary is determined by using the empirical correlation proposed by Mundo et al. (1995) as follows:

$$K = Oh\, Re^{1.25} = 57.7 \tag{4}$$

where K is dimensionless parameter for impingement, expressed in terms of Reynolds and Ohnesorge numbers which are defined as $\rho_d D_b v_{bn}/\eta_d$ and $\eta_d/\sqrt{\rho_d \sigma_d D_b}$, respectively. Also, η_d represents the viscosity of the droplet. For the formulation of the splashing droplet behavior, the first step is to determine the mass of the splashed droplets. For a wetted surface, the ratio of the splashed mass to the mass of the incident droplet is determined by using the work of Bai and Gosman (1995) as follows:

$$r_m = \frac{m_s}{m_i} = 0.2 + 0.9RN(0, 1) \tag{5}$$

where $RN(0, 1)$ is a random number distributed uniformly between 0 and 1. In the splash regime, the secondary droplet size and the number of ejected droplets are determined as follows:

$$D_a = C_w D_b \tag{6}$$

$$N_{eject} = 0.187We_{bn} - 4.45 \tag{7}$$

where C_w can be given as $(r_m/N_{eject})^{1/3}$ from the mass conservation law. The number of ejected droplets in a parcel can be given from the experimental data of Naber and Farrell (1993). Secondary velocity component of splashed droplets can be determined from the energy conservation law as follows:

$$0.5m_i V_i^2 + \pi\sigma_d D_b^2 - \int_0^{t_e}\int_{\forall_f} \Phi \, d\forall_f \, dt = 0.5m_s V_s^2 + \pi\sigma_d D_a^2 N_{eject} \tag{8}$$

where $\forall_f$ is the volume of the fluid when the droplet is flattened out in the shape of a disc, and

also m_i and m_s represent the mass of an incident droplet and splashed droplets, respectively. In the above equation, V_i and V_s are the total velocity of an incident droplet and splashed droplets, respectively. Also, t_e represents the life time of an incident droplet. The last term on the left-hand side represents the viscous dissipated energy and can be expressed as follows:

$$\int_0^{t_e}\int_{\forall_f} \Phi \, d\forall_f \, dt \approx \Phi \forall_f t_e \approx \eta_d \left(\frac{v_{bn}}{h_f}\right)^2 \forall_f \cdot t_e = \eta_d \left(\frac{v_{bn}}{h_f}\right)^2 \pi d_{sp}^2 h_f \cdot \frac{t_e}{4}. \tag{9}$$

where d_{sp} and h_f are the diameter and height of film disc, respectively. The main difference between the new model and the previous models involving the splashing effect is in the determination of the total velocity of droplets after impingement by using the newly derived relationship for the dissipated energy instead of the critical Weber number, deduced from the experimental consideration. Introducing γ_{max}, We_s^T, and We_i^T, into Eq. (8), we can obtain the relationship for the total velocity of ejected droplets as follows:

$$We_s^T = \frac{C_w We_i^T}{r_m} - \left(\frac{K_v C_w We_{bn} \gamma_{max}^4}{r_m Re_{bn}} - \frac{12 C_w}{r_m}\right) - 12 \tag{10}$$

where K_v is constant value of 4.5 and γ_{max} is defined as $(d_{sp}/D_b)_{max}$ which is the dimensionless parameter of the disc when splashing occurs. Also, We_s^T, and We_i^T, are Weber numbers based on the total velocity of the splashing and impinging droplet, respectively. We assume that the splash occurs at the moment of crown emergence and, therefore, adopt γ_{max} as 2.0 from the observation of Yarin and Weiss (1995). The second term on the right-hand side represents the dissipated energy of the droplet when the incident droplets impinge on the wall.

Next step is to determine the velocity components of ejected droplet. In the new model, we should determine the tangential component of the ejected droplets and then, from Eq. (10), the normal velocity and ejection angle of ejected droplets can be subsequently determined. Assuming that the tangential component of the droplet velocity after impingement can be approximated by the tangential velocity of the crown (a liquid sheet virtually normal to the wall), the position of the crown for a single-droplet impingement can be given from the theoretical relationship of Yarin and Weiss (1995) as follows:

$$\frac{r_c}{D_b} = \left(\frac{2}{3}\right)^{1/4} \frac{v_{bn}^{1/2}}{D_b^{1/4} h_f^{1/4}} (t - t_0)^{1/2} \tag{11}$$

where r_c and t_0 are the crown radius and the time for a droplet to create the initial spot in the center of the film, respectively. Finally, we can obtain the tangential velocity of ejected droplets from the above equation as follows:

$$\upsilon_f = \frac{0.452 K_f \cdot Re_{bn}^{1/8} \cdot \upsilon_{bn}}{\sqrt{\Psi}} \tag{12}$$

where Ψ represents the time fraction which is defined as the ratio of time when the splash occurs to the residence time of an incident droplet. In a physical sense, this time fraction may be affected by the kinematic parameter of an incident droplet. Therefore, in the present study,

the time fraction is derived as a function of the droplet Reynolds number.

$$\Psi = 1.0; \quad Re_{bn} \leq 577$$

$$\Psi = 0.204 Re_{bn}^{1/4}; \quad Re_{bn} > 577 \tag{13}$$

According to Yarin and Weiss (1995), the theoretical relationship is consistently overestimated. This is due to their exclusion of the momentum losses at the moment of impingement. To consider the effect of viscosity, we introduce the friction factor K_f, which is randomly chosen in the range between 0.81 and 0.91. Hence, from Eqs. (10) and (12), we can obtain the tangential and normal components of ejected droplet velocity. For three-dimensional calculations, it is necessary to determine the deflection angle ϕ. We can finally obtain the tangential component of ejected droplet velocities as follows:

$$v_{at,\,x} = v_{bt,\,x} + v_f \cos\phi \tag{14}$$

$$v_{at,\,y} = v_{bt,\,y} + v_f \sin\phi \tag{15}$$

where, ϕ is chosen stochastically by using the correlation proposed by Naber and Reitz (1988). Subscripts x and y denote the components of tangential velocity in the cartesian coordinate.

3. Numerical method

The gas phase is derived in terms of the Eulerian conservation equations and turbulent transport is modeled by the modified k–ε model. The droplet parcel equations of trajectory, momentum, mass and energy are written in Lagrangian form. To couple between the gas phase velocity and the pressure field, the implicit and non-iterative PISO algorithm is used in the present study. The gas phase transport equations are discretized by finite volume method. With this process, the Euler implicit method is used for the transient term, and a hybrid upwind/central difference scheme is used to approximate the convection and diffusion terms. The ordinary differential Lagrangian equations for the droplets are also discretized in the Euler implicit manner.

Droplets may become unstable under the action of the interfacial forces induced by their motion relative to the continuous phase. The present study incorporates a breakup model widely used for the breakup of liquid droplets in a gaseous stream proposed by Reitz and Diwakar (1987), where two breakup regimes are identified as the bag and stripping breakup. Also, the collision and coalescence model of O'Rourke and Bracco (1980) are used in this paper.

4. Results and discussion

In the present work, to assess the performance of three different models i.e. the models of Watkins and Wang (1990) and Park (1994), and the new model, we perform the calculations

Table 2
Specifications of test cases

Test cases	Test 1	Test 2	Test 3	Test 4
Wall distance (mm)	24	34	24	30
Trap pressure (bar)	15	15	15	1
Gas temperature (K)	293	293	293	293
Nozzle diameter (mm)	0.3	0.3	0.2	0.22
Injection pressure (bar)	140	140	138	260
Injection duration (ms)	1.2	1.2	1.3	1.0
Injection angle (°)	0	0	0	0
Fuel injected (mm^3/pulse)	10.5	10.5	8.3	4.0
Reference	Katsura et al. (1989)	Katsura et al. (1989)	Fujimoto et al. (1990)	Arcoumanis and Chang (1994)

for four different test cases as shown in Table 2. In particular, for test 4, the numerical simulation is performed in order to analyze the internal structure of wall sprays after impingement. Computational domain for all tests with a $50 \times 50 \times 40$ (x, y and z, respectively) grid is used, as shown in Fig. 1. This mesh arrangement is found to reduce the grid-size sensitivity of the results considerably. For all tests, a time step of 10 μs is adopted and for test 1, a total of 4000 droplet parcels are introduced throughout the injection duration time. Computing time for convergence is about 2.4 h for test 4 using CRAYC90 (YMP-SINGLE CPU) in the case of the new model.

To simulate the phenomena of impinging sprays on the wall, it is crucial to determine the initial droplet and injection velocity at the nozzle because these parameters have great influence on the numerical results. From test 1 to test 3, we assume that the initial size of droplets at the nozzle exit is equal to the nozzle diameter. This treatment is based on the assumption that atomization and droplet breakup are indistinguishable processes for high velocity and gas density, as pointed out by Reitz and Diwakar (1987). However, for the low gas density of test 4, the above assumption may cause the impinging droplet size to be exaggerated as referred by Reitz and Diwakar (1987). Hence, it is assumed as shown in Fig. 2 that the initial size of droplets is determined by using a Gaussian distribution with the Sauter Mean Diameter (SMD) of 40 μm. This value is given from experimental results, in which the SMD at the centerline of the free spray at a 30 mm distance from the nozzle exit is about 40 μm. The schedule of injection velocity for the tests 1, 2 and 4 can be determined by the curve-fitted relationship from the experimental data (Katsura et al., 1989; Arcoumanis and Chang, 1994). However, injection velocity for test 3 is assumed by constant velocity because there are no known information in the Ref. (Fujimoto et al., 1990).

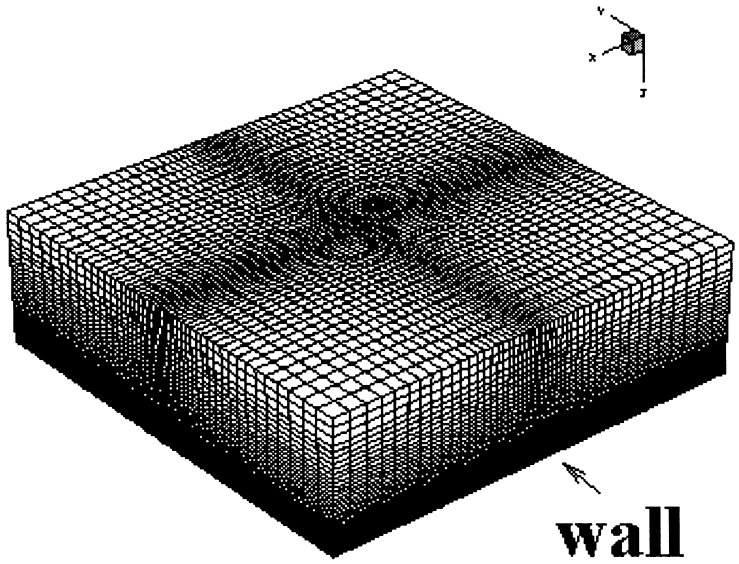

Fig. 1. Grid generation of the present study.

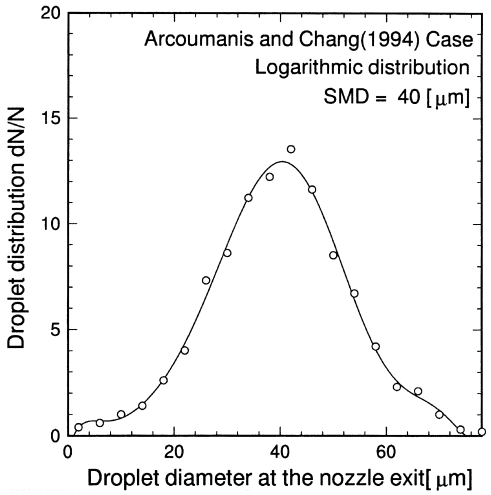

Fig. 2. Initial droplets size at the nozzle exit (Test 4).

4.1. Overall structure of wall spray (test 1, 2 and 3)

To begin with, we analyze the overall structure of the wall spray, i.e. radius and height of wall spray, for high gas density. Katsura et al. (1989) conducted experiments in which a single spray has normally impinged on a flat plate at high pressure and room temperature. Fig. 3(a) and (b) show the predicted spray pattern for test 1 at 0.7 ms and 1.5 ms after injection start. Figs. 4 and 5 compare the temporal behavior of the wall spray radius and height for test 1 and test 2. For these comparisons, the computed spray radius and height are defined as the distance from the impingement site and the wall surface, respectively, to the droplets which lie in the computational domain. The radius and height of wall sprays are automatically determined in the developed code. As shown in these figures, the new model shows the good agreement with the experimental data for the spray height. Maximum error of the new model is about 7.6 and 1.6% for test 1 and test 2 respectively, suggesting that the new model can predict the behavior of splashing droplets effectively. On the other hand, we can see the models of Watkins and Wang (1990) and Park (1994) under-predict the spray height, especially at the early stage of injection start. This may be due to two reasons. First, the criterion between the rebound and splash regimes in these models is based on the critical Weber number of 80, determined by Wachters and Westerling (1966). Actually, as pointed out by Mundo et al. (1995), for Weber numbers larger than 80, the impinging droplet on a wetted wall may splash into some secondary droplets. However, according to the experimental consideration of Wachters and Westerling (1966), an incident droplet is spread in the tangential direction along the wall, as like the liquid jet. Therefore, for the case of the wetted and cold wall, it is not consistent to use the above criterion, coming from the experimental results of Wachters and Westerling (1966). Second, the velocity of splashed droplets in the previous models is determined by some relationships, obtained from experimental data on a hot wall above the Leidenfrost temperature of the fuel. Hence, for impinging droplets on the cold wall, these relationships may be inappropriate. Actually, in the models of Park (1994) and Watkins and Wang (1990),

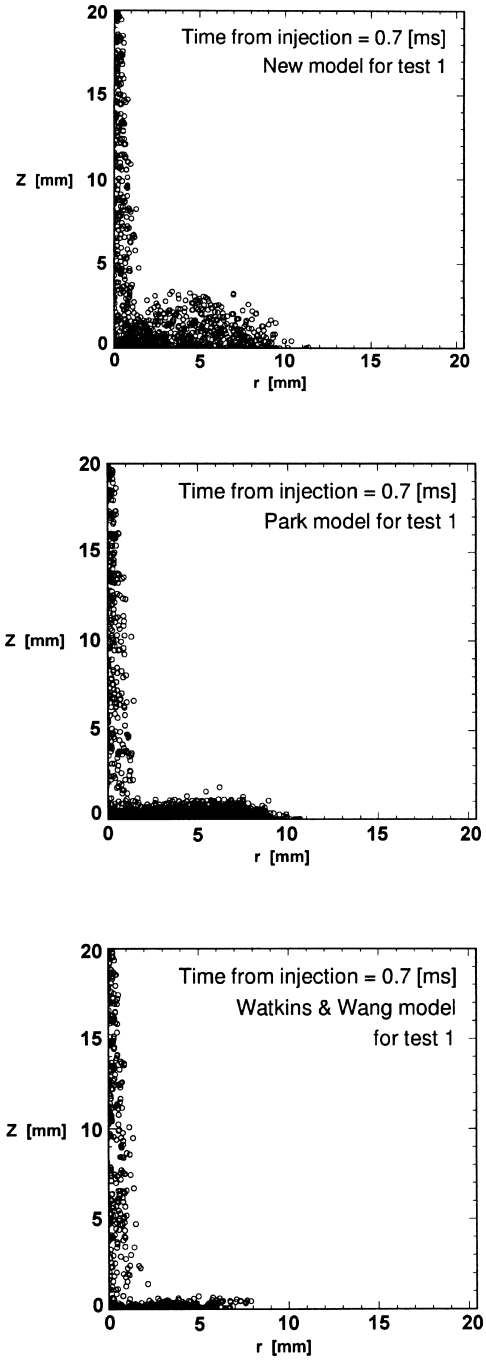

Fig. 3. (a) Calculated spray development using three different impingement models at 0.7 ms (Test 1). (b) Calculated spray development using three different impingement models at 1.5 ms (Test 1).

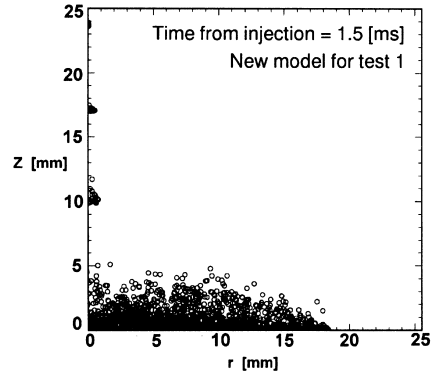

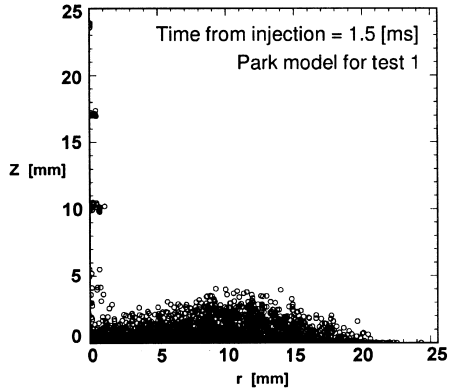

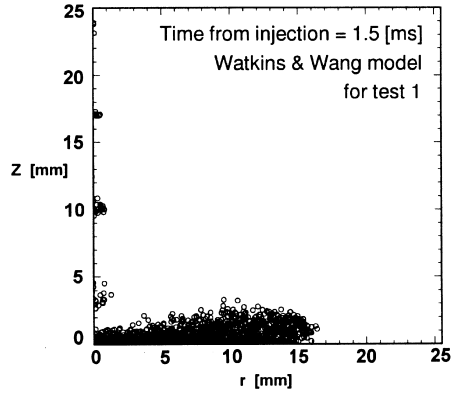

Fig. 3 (*continued*)

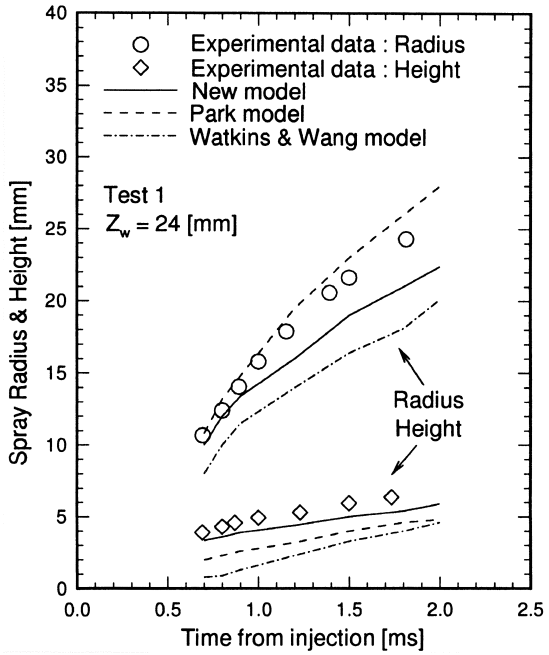

Fig. 4. Comparison of the predicted spray radius and height with the experimental data of Katsura et al. (1989) (Test 1).

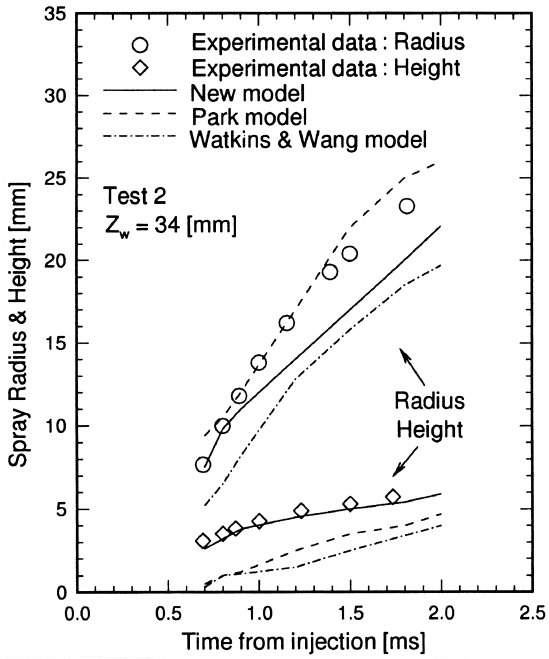

Fig. 5. Comparison of the predicted spray radius and height with the experimental data of Katsura et al. (1989) (Test 2).

the Weber number after impingement is assumed to be unity and zero, respectively, for the Weber number larger than 80. Despite of the fact that the Weber number of splashed droplets may be higher than 1 for the typical size of 20–30 μm in D1 engines, the Weber number of ejected droplets is so small that the previous models can not predict the correct behavior of droplets after impingement. Therefore, the assumptions used in the models of Park (1994) and Watkins and Wang (1990) are not appropriate for impinging sprays on the cold wall. It can be observed that, at the early stage after start of impingement, the new model and Park's model are in better agreement for the spray radius with the experimental data than the model of Watkins and Wang (1990). However, the new model under-predicts the spray radius at a later stage of injection. For the new model, the maximum error is about 12.1 and 11.6% occurring for test 1 and test 2, respectively, at the end of the injection period. This discrepancy is larger towards the end of injection, and is caused by the modeling of droplet size distribution after impingement. The distribution being involved in the new model is based on the experimental data of Naber and Farrell (1993). Park and Watkins (1996) pointed out that the distribution is reasonable for applying to diesel engines. But, for high Weber number, this may produce smaller droplets after impingement than those in the actual phenomena. Hence, smaller droplets can not penetrate in the radial direction effectively because of insufficient inertia of ejected droplets. Nevertheless, the reason why the radial penetration of Park model can be closer to experimental data may be the under-predicted normal velocity, resulting in producing smaller ejection angle. Therefore, the more suitable data for the size distribution of ejected droplets are required. Comparing test 1 with test 2, we can see that the spray radius decreases

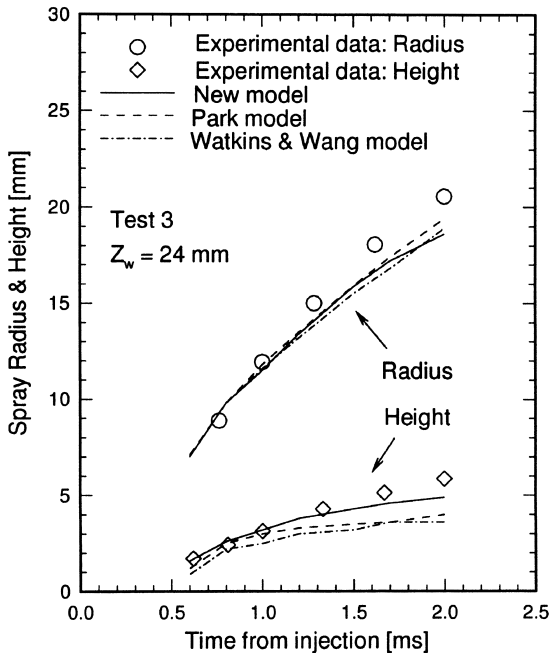

Fig. 6. Comparison of the predicted spray radius and height with the experimental data of Fujimoto et al. (1990) (Test 3).

as the impingement distance is increased, indicating that a longer time is needed for the spray to reach the wall prior to impingement.

Test 3 is very similar to test 1 and 2 in terms of experimental conditions, but in test 3 performed by Fujimoto et al. (1990), the higher injection velocity and smaller size of initial droplets at the exit of the nozzle cause different behavior of the impinging droplets on the wall than tests 1 and 2. High injection velocity can introduce smaller droplets into the calculation domain, and then smaller droplets after impingement penetrate away from the wall and the impingement site with lower inertia because the higher is the injection velocity, the smaller is the size of droplets after impingement. Hence, test 3 is different from tests 1 and 2 in spite of similar conditions. It can be seen in Fig. 6 that all of models show similar trends with the experimental data for spray radius, while the new model slightly under-predicts the spray radius with maximum error of about 9.5% at 2.0 ms after injection start. However, the new model gives excellent agreement with experimental data for the spray height.

4.2. Internal structure of wall spray (test 4)

The phenomenon of impinging spray on the wall can be affected by various factors such as atomization at the nozzle exit, the behavior of impinging droplets at the impingement site and the interaction between turbulent gas-phase flow and the dispersed droplets. These factors are recognized as one of the major parts of the two-phase flow. For the last ten years, most submodels have been assessed by comparing the overall structure such as the radius and height of the wall spray with experimental data. To give better understanding of the interaction between the gas-phase flow and the dispersed droplets, it is important to analyze the internal structure, i.e. droplet velocities, SMD and velocities of the gas-phase flow. Arcoumanis and Chang (1994) have investigated the spatial and temporal characteristics of transient diesel sprays impinging on unheated and heated wall using Phase Doppler Anemometer. In the present paper, we compare the results of three different models with experimental data of Arcoumanis and Chang (1994).

Fig. 7 shows the measuring locations, corresponding to representative regions of the two-phase wall-jet: the main wall-jet region (1), the stagnation region (2) and the downstream

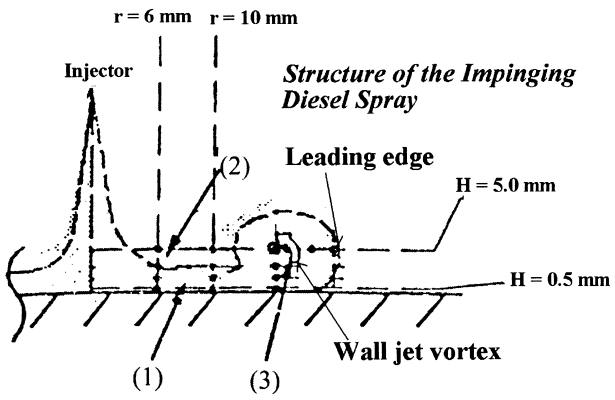

Fig. 7. Measuring locations (Test 4).

region (3). According to Katsura et al. (1989), the main wall-jet region lying in the inside of the impinged part, where the tangential velocity and momentum of the droplets are large. Also, in the stagnation region which lie in the edge of impinged part, droplets at the peripheral region are pushed out to the upper side, and then stagnate in this region and are overtaken by droplets near the wall. In the downstream region, wall jet vortex can be observed, and turbulent mixing between the droplets and surrounding gas occurs strongly. In the present study, the main wall-jet near the wall and stagnation region are only discussed here because regions (1) and (2) are mainly affected by the submodel, while the region (3) is much more affected by interaction between the turbulent flow and droplets than the submodel.

Figs. 8 and 9 represent the comparison of the predicted tangential velocities of droplets using the three models in the main wall-jet region ($r = 6$ mm, $H = 0.5$ mm) and near the stagnation region ($r = 6$ mm, $H = 5.0$ mm). The new model over-predicts the droplet tangential velocity, but produces similar trend in that the tangential velocity starts at a maximum and then gradually decays to approximately zero. The near-wall velocities are not settled to a quasi-steady state during the whole injection duration, contrary to those in the stagnation region. Near the wall ($r = 6$ mm and $H = 0.5$ mm), the new model shows better agreement with the experimental data than the models of Watkins and Wang (1990) and Park (1994). Also, it can be observed in these figures that, in general, the mean velocity decreases as the distance from the wall surface increases, suggesting that most of the droplet tangential momentum remains concentrated in the region near the wall surface. This trend is in good agreement with the experimental results of Arcoumanis and Chang (1994). However, in contrast to the experimental observation, the actual spray reaches a quasi-steady state slightly earlier than that

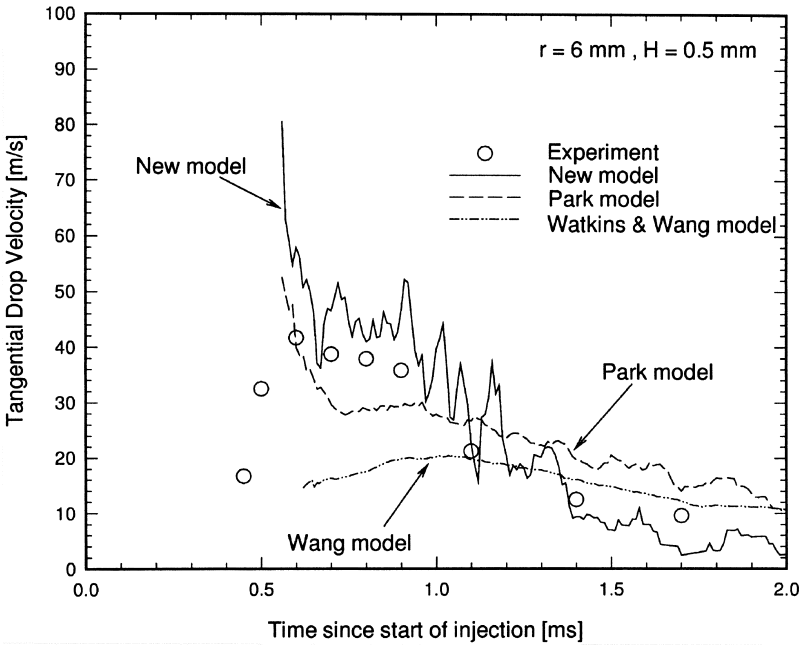

Fig. 8. Comparison of the predicted tangential droplet velocity with the experimental data of Arcoumanis and Chang (1994) at $r = 6$ mm and $H = 0.5$ mm (Test 4).

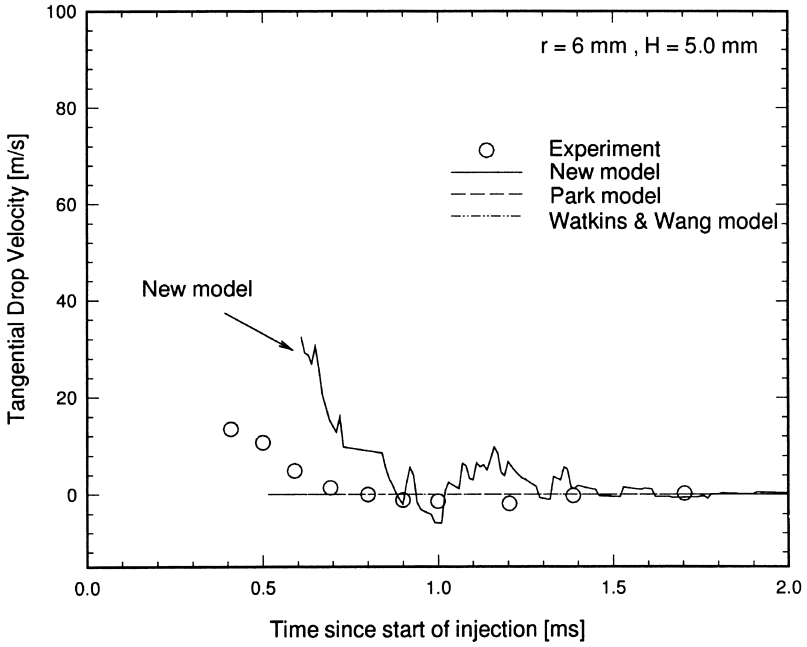

Fig. 9. Comparison of the predicted tangential droplet velocity with the experimental data of Arcoumanis and Chang (1994) at $r = 6$ mm and $H = 5.0$ mm (Test 4).

predicted by the new model which, however, predicts well the tangential velocity of the droplets near the stagnation region, while the previous models can not capture the existence of the ejected droplets in this region since these models do not effectively consider the splash effect.

Figs. 10 and 11 compare the predicted tangential velocity of the droplets in the main wall-jet region and near the stagnation region at $r = 10$ mm with the experimental data. Near the wall, there are some differences between the results of the new model and the experimental data after 1.0 ms. In addition, we can find that the Park's model over-predicts the tangential velocity of droplets after 1.0 ms. However, near the stagnation region ($H = 5.0$ mm), the new model is in better agreement with the experimental data than the previous models. In particular, the previous models do not find the presence of ejected droplets at the stagnation region($r = 10$ mm and $H = 5.0$ mm), while the new model captures the negative tangential velocities, indicating that a wall vortex exists in this region, despite the over-predicted velocities at the first stage of injection.

Figs. 12–15 show the SMD profiles at $r = 6$ and 10 mm and $H = 0.5$ and 5.0 mm. Arcoumanis and Chang (1994) have argued that, at $r = 10$ mm and $H = 0.5$ mm, there are some fluctuating curves during the whole injection period different from those upstream of the wall-jet, caused by the outcome of the competitive process between droplet breakup and coalescence. We can see that all models under-predict the SMD values relative to the experimental data. This problem may be due to the breakup and coalescence model near the wall, and inappropriate size distribution of the droplets after impingement. However, in the downstream and stagnation regions ($r = 10$ mm and $H = 5.0$ mm), the predicted SMDs using

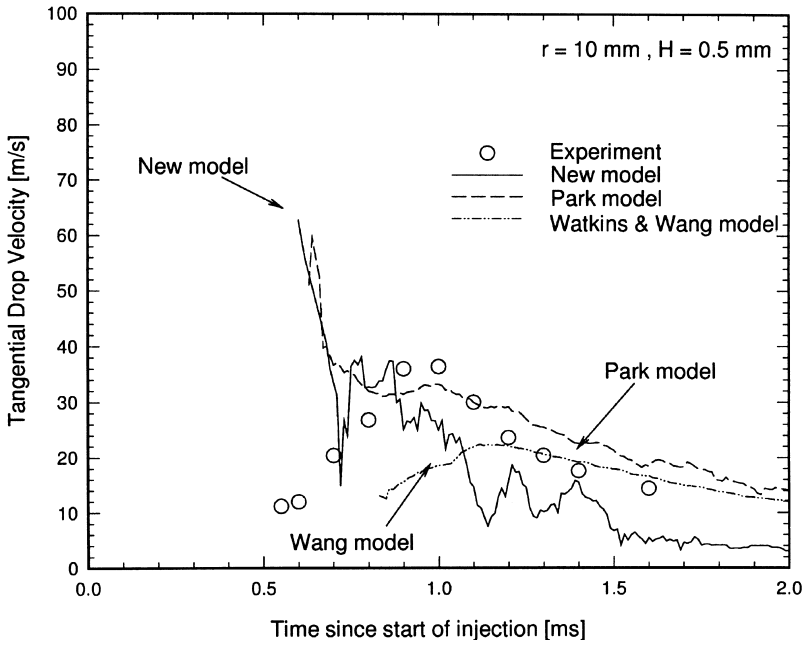

Fig. 10. Comparison of the predicted tangential droplet velocity with the experimental data of Arcoumanis and Chang (1994) at $r = 10$ mm and $H = 0.5$ mm (Test 4).

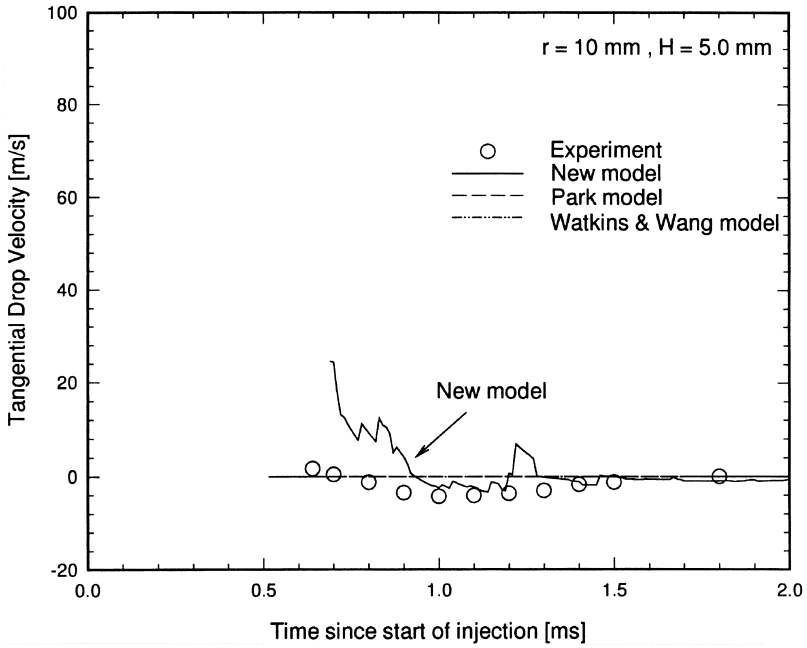

Fig. 11. Comparison of the predicted tangential droplet velocity with the experimental data of Arcoumanis and Chang (1994) at $r = 10$ mm and $H = 5.0$ mm (Test 4).

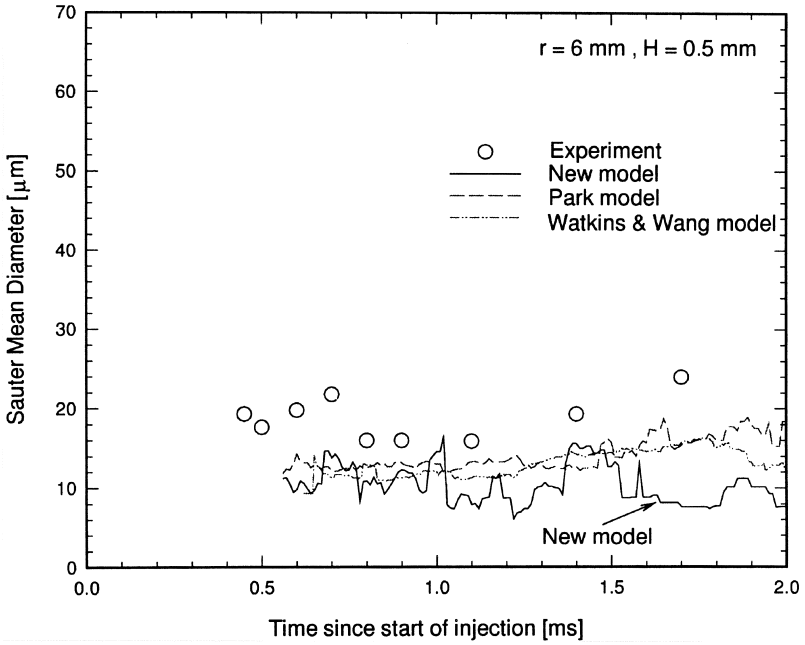

Fig. 12. Comparison of the predicted SMD profiles with the experimental data of Arcoumanis and Chang (1994) at $r = 6$ mm and $H = 0.5$ mm (Test 4).

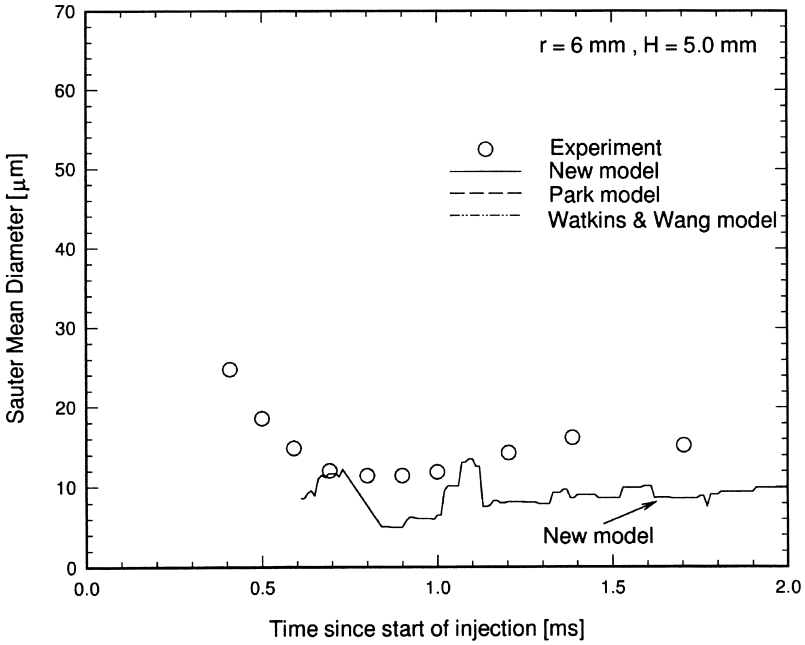

Fig. 13. Comparison of the predicted SMD profiles with the experimental data of Arcoumanis and Chang (1994) at $r = 6$ mm and $H = 5.0$ mm (Test 4).

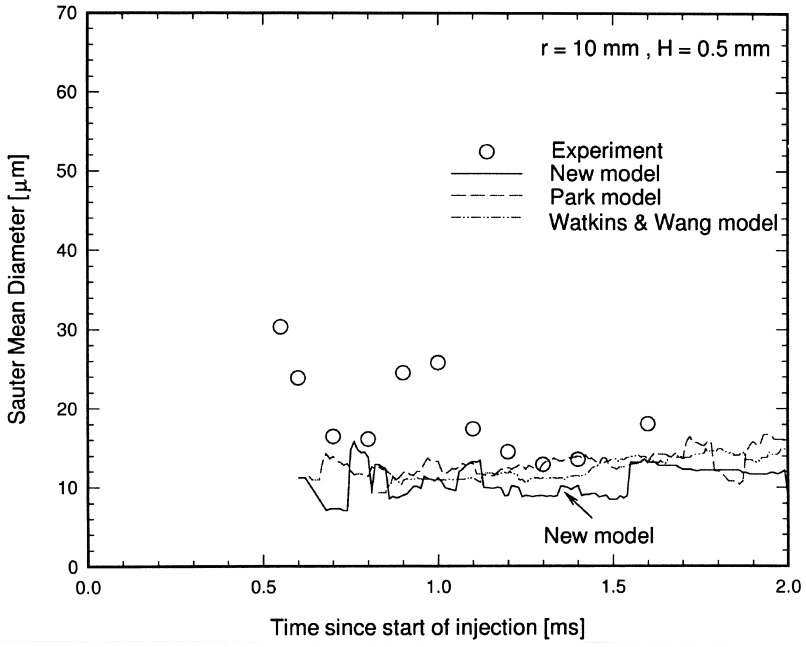

Fig. 14. Comparison of the predicted SMD profiles with the experimental data of Arcoumanis and Chang (1994) at $r = 10$ mm and $H = 0.5$ mm (Test 4).

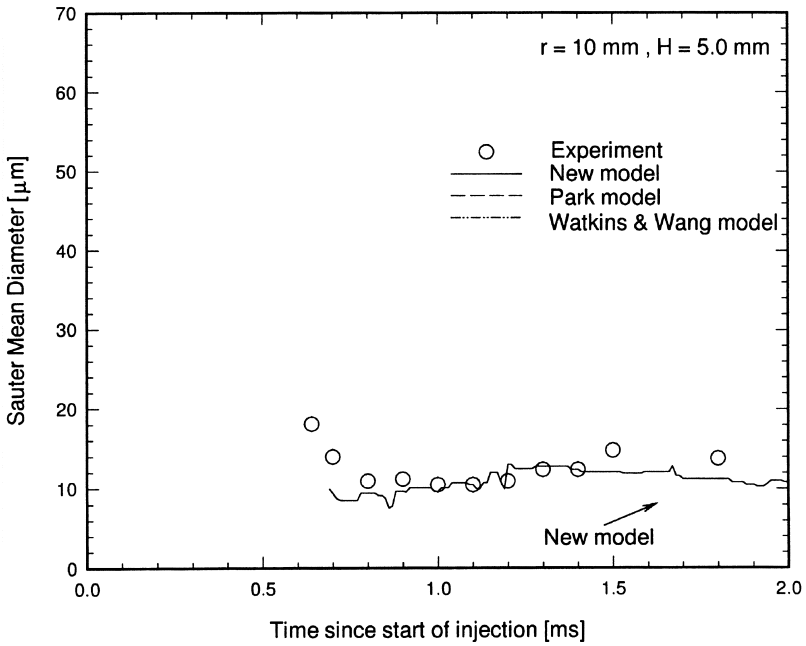

Fig. 15. Comparison of the predicted SMD profiles with the experimental data of Arcoumanis and Chang (1994) at $r = 10$ mm and $H = 5.0$ mm (Test 4).

the new model are in fairly good agreement except at the first stage of injection, while those of the previous models fail to predict the existence of ejected droplets.

Fig. 16 shows the transient behavior of the predicted flow velocity vectors at $r = 10$ mm and $H = 3.0$ mm, compared to the experimental data. According to the experiment, the first droplets pass through the measurement position, moving almost parallel to the wall. However, as the spray develops, the point in question first becomes part of the head vortex, so that the velocity vectors swing upwards away from the wall, and then downwards again, as the head vortex passes by. Finally, the vectors attain a steady-state position about 15° to the vertical axis where the flow is directed almost vertically downwards towards the wall, indicating that after 2.0 ms, air is essentially being entrained into the main wall-jet region. For all models, the overall trends are in good agreement with the experiment. Also, the time taken for the vector to settle to a steady-state position agrees well with the experiment, but for the previous models, the steady-state direction of the vector is about 0° to the vertical axis, while for the new model, that is about 18°, indicating that the new model is in better agreement with the experimental results than the previous models, i.e. at about 15°. The models of Park (1994) and Watkins and Wang (1990) predict a slower rotation rate in the 0.8–1.0 ms elapsed time period,

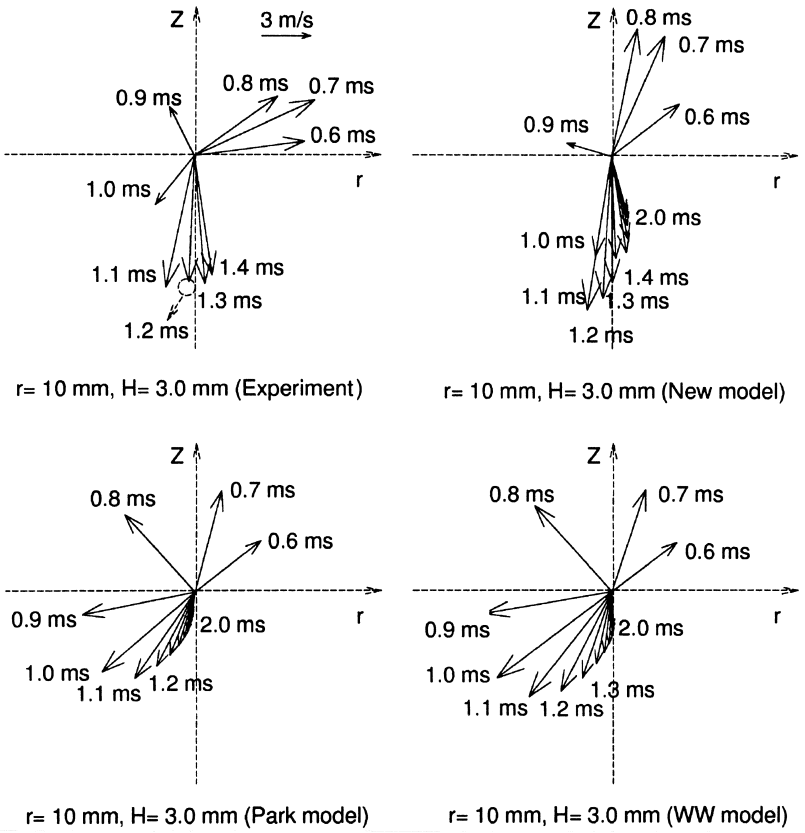

Fig. 16. Comparison of the predicted gas-phase velocity with the experimental data of Arcoumanis and Chang (1994) at $r = 10$ mm and $H = 3.0$ mm (Test 4).

suggesting that air entrainment into the actual spray is more vigorous than that predicted. This means that the predicted head vortex using the previous models is rarely being pushed past the measurement location. This failure of the previous models is probably due to the lack of dispersion of the predicted spray, as pointed out by Park and Watkins (1996). The new model gives the effective prediction of the rotational speed in the range from 0.8 to 1.0 ms. The reason why the new model can predict the rotational speed of the head vortex effectively is that, by including the splash effect, it can correctly represent the behavior of dispersed droplets away from the wall surface.

Figs. 17–19 compare the magnitude of the normal, tangential and total velocities of the gas-phase flow at $r = 10$ and $H = 3.0$ mm (near the stagnation region). Unlike the previous models, the measured slightly oscillatory trend is predicted by the new model. This is due to the characteristic of the new model where the ejection angle is arbitrarily determined by energy conservation law, contrary to the previous models where the angle is determined within a confined range because the normal velocities of the ejected droplets are relatively small.

In Fig. 17, the positive direction of the normal velocity is defined as the direction away from the wall. For the new model, the predicted time changing the velocity magnitude to a negative value is closer to the experimental data than the previous models, for which the predicted time is faster than measured. Physically, the existence of the region of negative velocities indicates that the surrounding gas is entrained into the main wall-jet region. Hence, it may be thought that the new model can effectively predict the magnitude of the entrained surrounding gas into the main wall-jet region especially after 1.0 ms, while the previous models can over-predict it. This suggests that the new model can reflect on the dispersion of droplets effectively.

As shown in Fig. 18, the predicted tangential velocities using the previous models are

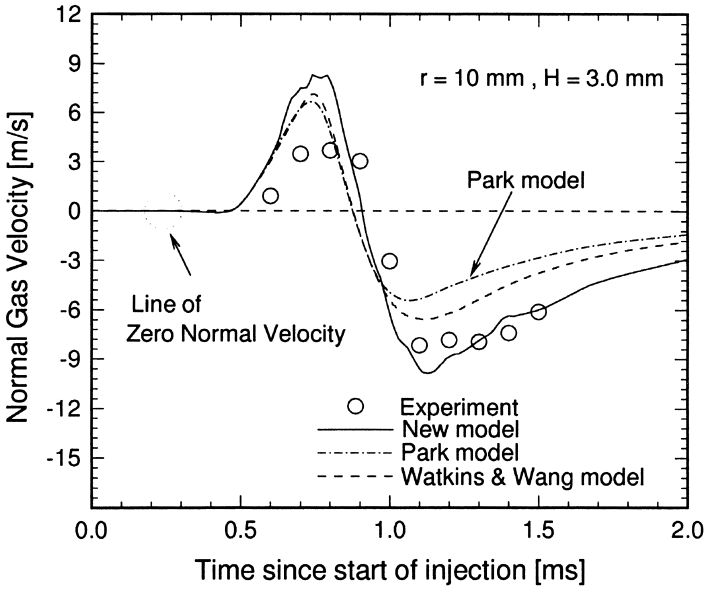

Fig. 17. Comparison of the predicted normal gas-phase velocity with the experimental data of Arcoumanis and Chang (1994) at $r = 10$ mm and $H = 3.0$ mm (Test 4).

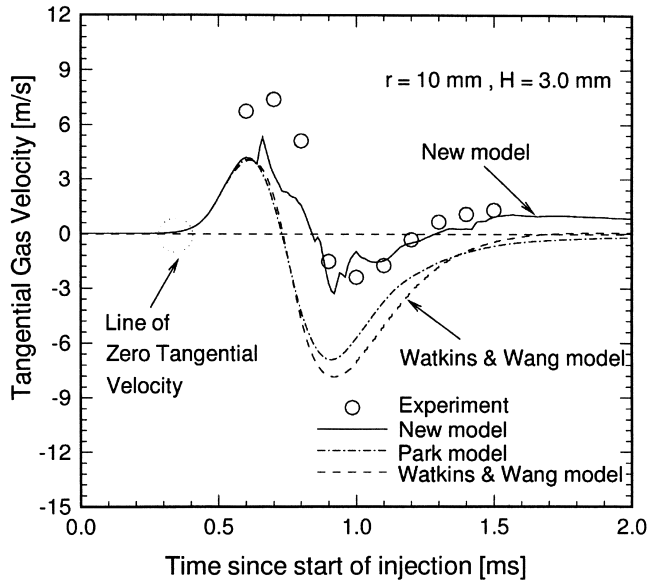

Fig. 18. Comparison of the predicted tangential gas-phase velocity with the experimental data of Arcoumanis and Chang (1994) at $r = 10$ mm and $H = 3.0$ mm (Test 4).

approaching zero earlier than results of the experiment and of the new model. This means that the previous models over-predict the rotational speed of head vortex at a point in question at early stage of injection, corresponding to previous results. This is probably due to lack of dispersion further away from the wall in the previous models, which suggests that the ejection angle after impingement is so small that the penetration is over-predicted outwards in the radial direction and then, near 0.8 ms at the early stage of injection, the rotational speed is

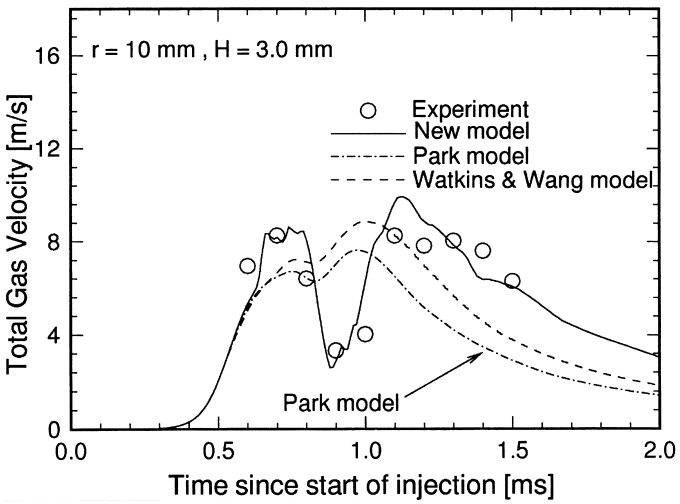

Fig. 19. Comparison of the predicted total gas-phase velocity with the experimental data of Arcoumanis and Chang (1994) at $r = 10$ mm and $H = 3.0$ mm (Test 4).

faster than that measured. Also, it can be noted that after 1.3 ms the previous models fail to predict that the tangential velocity becomes positive, indicating that during the last injection period, the rotational speed of the actual flow is faster than that predicted by the previous models. On the other hand, it can be seen that good agreement of the new model exists, suggesting that the new model can predict the temporal behavior of the head vortex effectively at the stagnation region.

Finally, Fig. 19 presents the measured and predicted magnitude of the total flow velocity at $r = 10$ mm and $H = 3.0$ mm. As seen in this figure, the new model gives good results, but neither of the models of Watkins and Wang (1990) and Park (1994) captures the minimum of the total velocities effectively. Physically, the occurrence of the minimum of the total flow velocity at a certain time indicates that the magnitude of the normal and tangential velocities become minimum at that time. Also, the center of the vortical structure can be determined by the position where the normal velocity is zero which allows the arrival time of the vortex center at a certain position in question to be estimated by identifying the time at which the normal velocity crosses the zero line. Through Figs. 17–19, it becomes clear that the new model can capture the time reaching the zero line or minimum value effectively, indicating that the model is capable of predicting the temporal behavior of the head vortex in impinging sprays.

5. Conclusions

A new submodel for spray/wall impingement was developed and tested against experimental data and the earlier models. Intrinsically, the previous models of Watkins and Wang (1990) and Park (1994) which have been based on the hot wall data are not capable of describing the splash mechanism because there are no physical bases on the splash mechanism in these models. The new model was developed in the present study to embody the splash mechanism physically, and was devised to represent the situations involving wall temperatures below the fuel boiling point on the basis of the conservation law and experimental considerations. The main feature of the new model is in the determination of the tangential and normal velocities after impingement. The derivation of the new formulae for the viscous dissipated energy of the film disc and the modification of the theoretical relationship are the main different parts from other previous models. To validate the new model, the spray flow was calculated using the new model and the earlier models of Watkins and Wang (1990) and Park (1994) for various experimental conditions. The following conclusions consist of two parts: one for the overall structure, and the other for the internal structure.

5.1. Overall structure of the wall spray

Numerical calculations for impinging sprays injected into the high pressure chamber were performed in tests 1, 2 and 3 where the overall structure of impinging sprays has been analyzed. The predicted spray height and radius using the new model and the previous models have been compared with the experimental data. The new model produced better prediction of the spray height although there were some errors in predicting the spray radius, while the

previous models under-predicted the spray height since these models could not account for the physics of the splash phenomenon. Consequently, the new model is more suitable for prediction of the overall structure of the wall spray than the earlier models.

5.2. Internal structure of the wall spray

Analysis of the test 4 was performed to obtain more detailed information about the internal structure of the wall spray. The droplet velocities and local droplet sizes at various measurement locations were compared with the experimental data of Arcoumanis and Chang (1994). The earlier models of Park (1994) and Watkins and Wang (1990) could not capture the presence of the ejected droplets in the stagnation region because these models can not describe the splash mechanism effectively. However, the new model predicted the existence of ejected droplets in the stagnation region and showed similar trend with the experimental results. Especially, the new model has made good predictions of the mean gas-phase velocities.

Through the above analysis, it can be concluded that the new model performs better in predicting the internal and overall structures of the wall spray, indicating that the model can effectively account for the impingement phenomena. In other word, it can be thought that the new model is physically more reasonable than the earlier models used in this article. In order to predict the structure of impinging spray on the wall more effectively, the more accurate size distribution of ejected droplets after impingement is needed and the more elaborate improvements of the new model are required.

Acknowledgements

The authors would like to acknowledge the financial support from SERI Supercomputer Center through CRAY R and D Grant Program.

References

Arcoumanis, C., Chang, J.C., 1994. Flow and heat transfer characteristics of impinging transient diesel sprays. SAE940678.

Bai, C., Gosman, A.D., 1995. Development of methodology for spray impingement simulation. SAE950283.

Eckhause, J.E., Reitz, R.D., 1995. Modeling heat transfer to impinging fuel sprays in direct-injection engines. Atomization and Sprays 5, 213–242.

Fujimoto, H., Senda, J., Nagae, M., Hashimoto, A., Saito, M., Katsura, N., 1990. Characteristics of a diesel spray impinging on a flat wall. In: Proc. COMODIA 90 Int. Symposium on Diagnostics and Modeling of Combustion in I.C. Engines, Kyoto, Japan, 193–198.

Gonzalez, M.A., Borman, G.L., Reitz, R.D., 1991. A study of diesel cold starting using both cycle analysis and multidimensional calculations. SAE910180.

Katsura, N., Saito, M., Senda, J., Fujimoto, H., 1989. Characteristics of a diesel spray impinging on a flat wall. SAE890264.

Matsumoto, S., Saito, S., 1970. On the mechanism of suspension of particles in horizontal conveying: Monte Carlo simulation based on the irregular bouncing model. J. Chem. Engng. Japan 3, 83–92.

Mundo, C., Sommerfeld, M., Tropea, C., 1995. Droplet-wall collisions: experimental studies of the deformation and breakup process. Int. J. Multiphase Flow 21, 151–173.

Naber, J.D., Farrell, P., 1993. Hydrodynamics of droplet impingement on a heated surface. SAE930919.

Naber, J.D., Reitz, R.D., 1988. Modeling engine spray/wall impingement. SAE880107.

O'Rourke, P.J., Bracco, F.V., 1980. Modeling of drop interactions in thick sprays and a comparison with experiment. In: Stratified Charge Automative Engines Conference, IMechE.

Park, K., 1994. Development of a non-orthogonal-grid computer code for the optimization of direct-injection diesel engine combustion chamber shapes. Ph.D. thesis, UMIST, UK.

Park, K., Watkins, A.P., 1996. Comparison of wall spray impaction models with experimental data on drop velocities and sizes. Int. J. Heat and Fluid Flow 17, 424–438.

Reitz, R.D., Diwakar, R., 1987. Structure of high-pressure fuel sprays. SAE870598.

Stanton, D.W., Rutland, C.J., 1996. Modeling fuel film formation and wall interaction in diesel engines. SAE960628.

Watkins, A.P., Wang, D.M., 1990. A new model for diesel spray impaction on walls and comparison with experiment. In: Proc. COMODIA 90 Int. Symposium on Diagnostics and Modeling of Combustion in I.C. Engines, Kyoto, Japan, 243–248.

Wachters, L.H.J., Westerling, N.A.J., 1966. The heat transfer from a hot wall to impinging water drops in a spherical state. Chem. Eng. Sci 21, 1047–1056.

Winterbone, D.E., Yates, D.A., Clough, E., Rao, K.K., Gomes, P., Sun, J.H., 1994. Quantitative analysis of combustion in high-speed direct injection diesel engines. In: Proc. COMODIA 94, Int. Symposium on Diagnostics and Modeling of Combustion in I.C. Engines, Yokohama, Japan, 261–267.

Yarin, A.L., Weiss, D.A., 1995. Impact of drops on solid surfaces: self-similar capillary waves, and splashing as a new type of kinematic discontinuity. J. Fluid Mech 283, 141–173.